Available online at www.sciencedirect.com
SCIENCE DIRECT
Journal of Power Sources 156 (2006) 345–354
JOURNAL OF POWER SOURCES
www.elsevier.com/locate/jpowsour

Development of PtRu-CeO_2/C anode electrocatalyst for direct methanol fuel cells

J.W. Guo, T.S. Zhao *, J. Prabhuram, R. Chen, C.W. Wong

Department of Mechanical Engineering, The Hong Kong University of Science and Technology, Clear Water Bay, Kowloon, Hong Kong SAR, China

Received 10 April 2005; accepted 20 May 2005
Available online 9 August 2005

Abstract

Ceria (CeO_2)-modified PtRu/C catalysts with different compositions of Ru and CeO_2, viz. $PtRu_{0.9}(CeO_2)_{0.1}$/C, $PtRu_{0.7}(CeO_2)_{0.3}$/C and $PtRu_{0.5}(CeO_2)_{0.5}$/C and unmodified PtRu/C catalyst were synthesized by the sodium borohydride reduction method. Transmission electron microscopic results indicated that the lower concentrated CeO_2-modified PtRu/C catalysts had almost a similar morphological structure (well-dispersed particles with size around 2.3–2.5 nm) with that of the unmodified PtRu/C catalyst. X-ray diffraction and X-ray photoelectron spectroscopy analyses indicated the formation of PtRu alloy and presence of CeO_2 in an amorphous form with a mixed oxidation states (Ce^{3+}–Ce^{4+}). Electro-catalytic activity of these catalysts for methanol oxidation was investigated by linear sweep voltammetry and chronoamperometry and it was found that the $PtRu_{0.7}(CeO_2)_{0.3}$/C catalyst yielded the higher methanol oxidation current than did the unmodified PtRu/C catalysts.

Keywords: CeO_2-modified PtRu/C catalysts; X-ray diffraction; X-ray photoelectron spectroscopy; Voltammetry; Methanol oxidation

1. Introduction

There has been a growing interest in the development of direct methanol fuel cells (DMFCs) because when compared with hydrogen-feed polymer electrolyte fuel cells (PEMFCs), DMFCs offer many advantages, such as higher energy density and much more compact system and lower weight [1–7]. However, the poor kinetics of the methanol oxidation reaction on the anode and the oxygen reduction reaction on the cathode remains as one of the most challenging problems for the wide-spread commercialization of DMFCs. On the anode, it is well known that the formation of CO intermediate species on the Pt sites during the methanol oxidation reaction creates an overpotential, which reduces the efficiency of the cell. According to the bi-functional mechanism, the CO intermediate species formed on the Pt sites can be oxidized by active oxygen atoms formed on the second metal of the bimetallic catalysts, such as PtRu [8–10], PtSn [10–12] and PtMo [13]. Among these bimetallic catalysts, PtRu exhibits the best performance. However, the use of the PtRu catalyst still cannot completely eliminate the CO species, which prevents complete oxidation of methanol to CO_2. Therefore, the improvement in the electro-catalytic activity of the PtRu catalyst is required to reduce or completely eliminate the CO intermediate species. To this end, some previous investigators, for example Lasch et al. [14] and Jusys et al. [15], modified unsupported PtRu catalysts by adding some transition metal oxides, such as MoO_x, VO_x and WO_x for the methanol oxidation; they demonstrated that these modified catalysts yielded a higher methanol oxidation current than did conventional PtRu catalysts. Similarly, Yang et al. [16] prepared a high surface area $PtRuWO_x$/C catalyst for the methanol oxidation reaction. They observed that the $PtRuWO_x$/C catalyst exhibited a higher activity than did the PtRu/C catalyst. In an another approach, Park et al. [17] fabricated sputtered PtRu and PtRu-WO_x nanocomposite thin film electrodes for the methanol oxidation reaction; their electrochemical testing

* Corresponding author. Tel.: +852 2358 8647; fax: +852 2358 1543.
E-mail address: metzhao@ust.hk (T.S. Zhao).

0378-7753/$ – see front matter © 2005 Elsevier B.V. All rights reserved.
doi:10.1016/j.jpowsour.2005.05.093

results indicated that the PtRu-WO_x nanocomposite electrode had a higher activity than did the PtRu thin film electrode. From the above-mentioned studies, it is clear that an addition of transition metal oxides (MoO_x, VO_x and WO_x) to PtRu enhanced methanol oxidation reaction. Further, it is interesting to mention that recently, Xu and Shen [18] showed higher ethanol oxidation current by using the CeO_2-modified Pt/C catalyst when compared with the Pt/C catalyst in alkaline medium.

In the present investigation, we employed CeO_2 as a co-catalytic material along with the PtRu bimetallic catalyst based on the fact that CeO_2 has the higher oxygen storage capacity (OSC) [19]. The oxygen atoms present in the lattice of CeO_2 can either be directly or indirectly involved in promoting the bi-functional mechanism of methanol oxidation reaction on the PtRu/C catalyst. Accordingly, we synthesized PtRu-CeO_2/C nanocatalysts with different compositions of Ru and CeO_2, viz. $PtRu_{0.9}(CeO_2)_{0.1}$/C, $PtRu_{0.7}(CeO_2)_{0.3}$/C and $PtRu_{0.5}(CeO_2)_{0.5}$/C. The electro-catalytic activity of the CeO_2-modified PtRu/C catalysts towards the methanol oxidation reaction was examined by using the linear sweep voltammetry (LSV) and chronoamperometry. We found that the $PtRu_{0.7}(CeO_2)_{0.3}$/C catalyst exhibited a higher activity for the methanol oxidation reaction than did conventional PtRu/C catalysts.

2. Experimental

2.1. Preparation of $PtRu_x(CeO_2)_{(1-x)}$/C nanocatalysts

20 wt.% $PtRu_x(CeO_2)_{(1-x)}$/C nanocatalysts ($x = 0$, 0.5, 0.7 and 0.9) were prepared according to the procedure reported elsewhere [20,21]. Briefly, these catalysts were prepared by maintaining the molar ratio of citric acid (CA) to platinum, ruthenium and cerium metal salts (PtCe:CA and PtRuCe:CA) at 1:1 in ammonium hydroxide solution (28–30 wt.%, Fisher). To these mixtures, an appropriate amount of Vulcan XC-72 carbon (E-TEK) was added and ultrasonicated for 30 min. Then, these mixtures were stirred at 50 °C for 10 h by constantly adding the ammonium hydroxide in order to maintain its volume in the mixtures. Subsequently, excess quantities of 0.1 M $NaBH_4$ (Merk) reducing agent were added, drop by drop, to the mixtures with vigorous stirring. After that, the mixtures were stirred for 3 h at room temperature. Then, the mixtures were filtered, washed with excess DI water and dried in a vacuum oven at 75 °C for 2 h. For comparison, 20 wt.% PtRu(1:1)/C and 20 wt.% CeO_2/C catalysts were also prepared. The 20 wt.% PtRu(1:1)/C catalyst was prepared by maintaining the molar ratio of CA to platinum and ruthenium (PtRu:CA) at 1:1 in ammonium hydroxide solution. The subsequent preparative procedures were maintained similar to that of the $PtRu_x(CeO_2)_{(1-x)}$/C catalysts as mentioned above. The 20 wt.% CeO_2/C was prepared by mixing an appropriate amount of cerium nitrate, CA and carbon in an ammonium hydroxide solution (molar ratio of cerium nitrate/CA was maintained at 1:1). Finally, all the catalysts were annealed at 400 °C under N_2 for 2 h to remove the CA stabilizer from the catalytic particles.

2.2. Physico-chemical characterization

High and low magnification transmission electron microscope (HMTEM and LMTEM) images were obtained by using a high-resolution JEOL 2010 TEM system operated with a LaB6 filament at 200 kV. The X-ray diffraction (XRD) patterns of the CeO_2/C, $PtCeO_2$/C, PtRu/C and $PtRuCeO_2$/C nanocatalysts loaded on carbon were obtained with a Philips Powder Diffraction System (model PW 1830) using a Cu Kα source operated at 40 keV at a scan rate of $0.025^\circ\ s^{-1}$. The X-ray photoelectron spectroscopy (XPS) measurements of the $PtCeO_2$/C, PtRu/C and $PtRuCeO_2$/C nanocatalysts were carried out with a Physical Electronics PHI 5600 multi-technique system using an Al monochromatic X-ray at a power of 350 W. The regional spectra were obtained by passing energies of 187.85 and 23.5 eV. The regional XPS of Pt4f and $Ru3p_{3/2}$ spectra were deconvoluted by using the multipak software to identify different oxidation states of Pt and Ru on carbon.

2.3. Electrochemical characterization

Electrochemical measurements were carried out by voltammetry using a potentiostat (EG&G Princeton, Model 273A). A conventional, three-electrode cell, consisting of glassy carbon (GC) with an area 0.125 cm^2 as the working electrode, Pt wire as the counter electrode and saturated calomel electrode (SCE) as the reference electrode, was used. A quantity of 40 μL catalyst ink was dispersed on the top surface of the GC over which 10 μL of 0.1 wt.% Nafion was added. Subsequently, the electrode was dried at 80 °C to yield a catalyst loading of 160 $\mu g\ cm^{-2}$. The voltammetry experiments were performed in 0.5 M H_2SO_4 solution containing methanol and without methanol at a scan rate of 50 $mV\ s^{-1}$. All the solutions were prepared by using ultrapure water (Millipore, 18 MΩ). N_2 gas was purged for nearly 30 min before starting the experiment. In all the experiments, stable voltammogram curves were recorded after scanning for 10 cycles. The chronoamperometry (current versus time response) tests were conducted using a three-electrode cell in 0.5 M H_2SO_4 solution containing 2 M CH_3OH at 0.4 V for the period of 2000 s.

3. Results and discussion

3.1. TEM analysis

Fig. 1 presents the TEM images of the PtRu/C, CeO_2-modified PtRu/C and Pt/C nanocatalysts. For the PtRu/C catalyst, as can be seen from the TEM image (Fig. 1a), well-dispersed PtRu nanoparticles around 2.5 nm in size

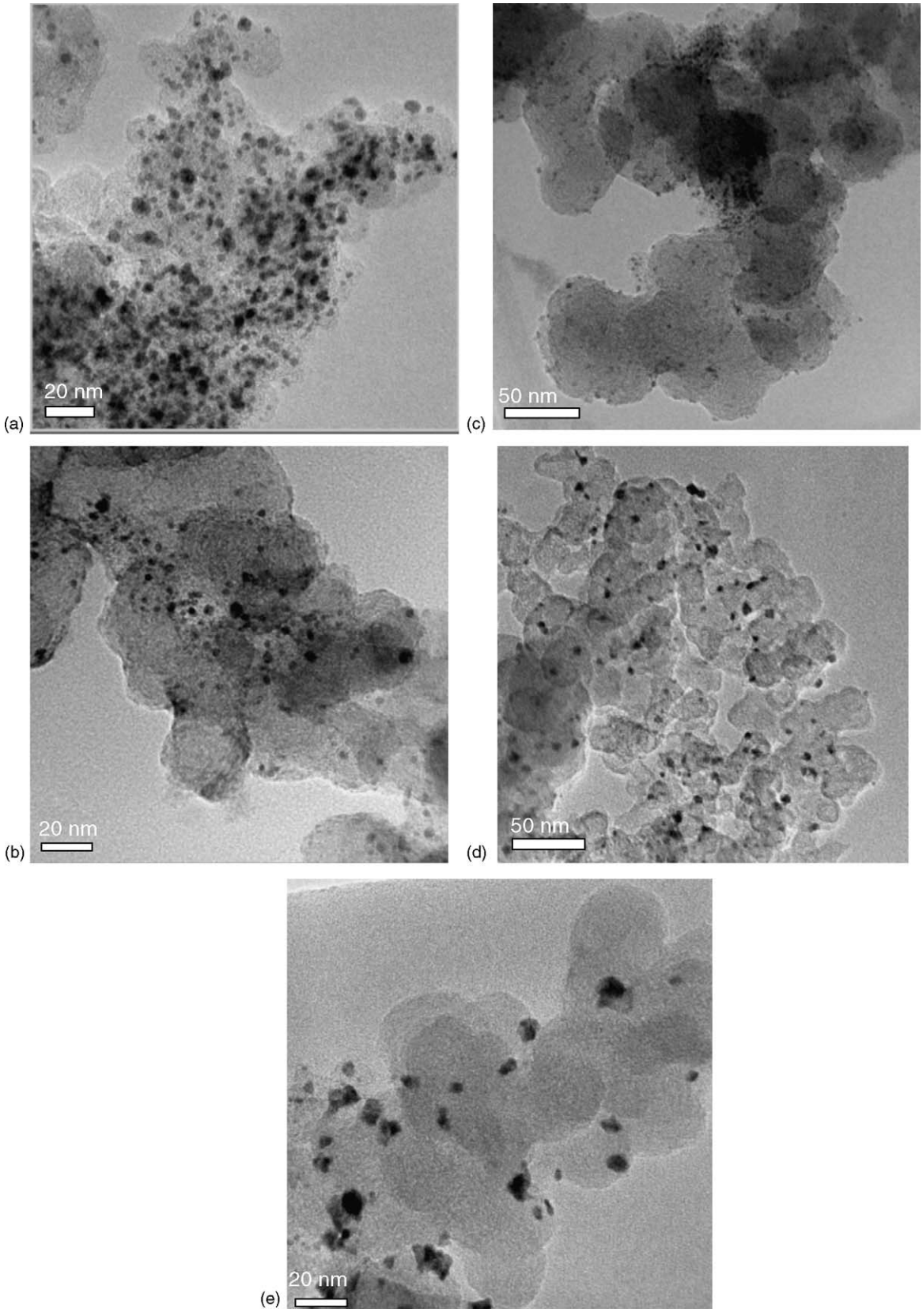

Fig. 1. TEM images of: (a) PtRu/C; (b) $PtRu_{0.9}(CeO2)_{0.1}$/C; (c) $PtRu_{0.7}(CeO2)_{0.3}$/C; (d) $PtRu_{0.5}(CeO2)_{0.5}$/C; (e) $Pt(CeO_2)$/C catalysts.

were formed on the carbon support. Similarly, for the CeO_2-modified PtRu/C catalysts, the well-dispersed nanoparticles were formed on the carbon support. For instance, in the $PtRu_{0.9}(CeO_2)_{0.1}$/C and $PtRu_{0.7}(CeO_2)_{0.3}$/C catalysts, the nanoparticles of size around 2.5 and 2.3 nm are formed, respectively (see Fig. 1b and c). However, for the higher concentrated CeO_2-modified PtRu/C ($PtRu_{0.5}(CeO_2)_{0.5}$/C) catalyst, although the particles are well-dispersed, they became relatively larger (around 5 nm) as shown in Fig. 1d. In the case of CeO_2-modified Pt/C catalyst, very big particles (6–10 nm) were formed that are scarcely dispersed on the carbon support (see Fig. 1e). From the above results, it appears that the 1:1 molar ratio (CA/PtRuCe and CA/PtCe) maintained for the preparation of higher concentrated CeO_2-modified PtRu/C and Pt/C nanocatalysts may not be an optimal ratio in controlling the growth of the particles. This might be due to the difference in the stabilization effect provided by CA over the different metal particles on the carbon support. The detailed discussion of this phenomenon is beyond the scope of the present work and further investigation is required.

3.2. XRD analysis

Fig. 2 shows the XRD patterns of CeO_2/C, $PtCeO_2$/C, PtRu/C, $PtRu_{0.9}(CeO_2)_{0.1}$/C $PtRu_{0.7}(CeO_2)_{0.3}$/C and $PtRu_{0.5}(CeO_2)_{0.5}$/C catalysts. CeO_2/C exhibits the characteristic diffraction peaks of (1 1 1), (2 0 0) and (3 1 1) at 2θ values of 28.5°, 46.6° and 55.7°, respectively. These values are in good agreement with the results reported in the literature [22]. The very broad nature of these peaks indicates that the CeO_2 is present in an amorphous phase. For $PtCeO_2$/C, the diffraction peaks responsible for the face-centered cubic (FCC) structure of Pt, that is, the (1 1 1), (2 0 0) and (2 2 0) peaks appeared at 2θ values of 39.7°, 46.3° and 67.45°, which are similar to the XRD pattern of the Pt/C catalyst [20,23]. In the case of the PtRu/C catalyst, the diffraction peaks are slightly shifted to higher 2θ values (40.3°, 46.7° and 68.1°), suggesting the formation of PtRu alloy with the

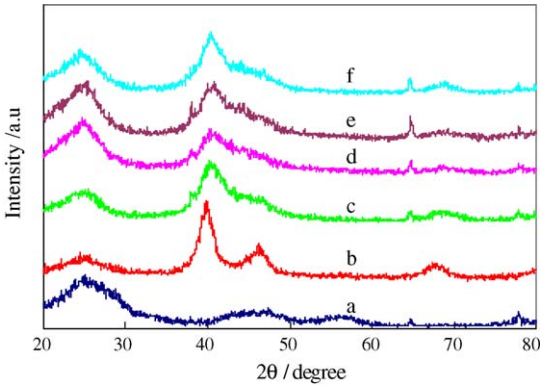

Fig. 2. XRD patterns of: (a) CeO_2/C; (b) Pt(CeO_2)/C; (c) PtRu/C; (d) $PtRu_{0.9}(CeO_2)_{0.1}$/C; (e) $PtRu_{0.7}(CeO_2)_{0.3}$/C; (f) $PtRu_{0.5}(CeO_2)_{0.5}$/C catalysts.

FCC structure. For $PtRu_{0.9}(CeO_2)_{0.1}$/C, $PtRu_{0.7}(CeO_2)_{0.3}$/C and $PtRu_{0.5}(CeO_2)_{0.5}$/C, the broad diffraction peaks appear in 2θ values, which is the same as that of the PtRu/C catalyst. The formation of broad peaks in all the CeO_2-modified PtRu catalysts indicated the presence of smaller PtRu particles. Moreover, in the XRD patterns of the CeO_2-modified Pt and PtRu catalysts, the peaks associated with the fluorite structure of pure CeO_2 did not appear prominently. This might be due to the presence of amorphous nature of CeO_2 particles in these catalysts. The above results show that the smaller PtRu alloy particles were formed and they might be sparingly covered by the amorphous CeO_2 particles in the CeO_2-modified PtRu/C catalysts.

3.3. XPS analysis

The surface compositions and chemical oxidation states of Pt, Ru and Ce in the CeO_2-modified PtRu/C nanocatalysts were determined by XPS analysis. Figs. 3 and 4 show the regional XPS spectrums of $Pt4f_{7/2}$ and $Ru3p_{3/2}$ for the $PtRu_{0.9}(CeO_2)_{0.1}$/C, $PtRu_{0.7}(CeO_2)_{0.3}$/C and $PtRu_{0.5}(CeO_2)_{0.5}$/C catalysts. These regional spectrums were deconvoluted and the results are summarized in Table 1. From Table 1, it is clear that the Pt is mainly present in its metallic state (about 67–84 at.%) as indicated by the $Pt4f_{7/2}$ peaks located at binding energy (BE) values of 71.85, 71.78 and 71.67 eV, respectively, for the $PtRu_{0.9}(CeO_2)_{0.1}$/C, $PtRu_{0.7}(CeO_2)_{0.3}$/C and $PtRu_{0.5}(CeO_2)_{0.5}$/C catalysts (see Fig. 3a–c). The slightly higher BE values noted for all the $Pt4f_{7/2}$ peaks of metallic Pt might be due to the greater dispersion of smaller Pt particles on the carbon support [24]. On considering the deconvoluted $Ru3p_{3/2}$ spectrums, nearly about 71.0, 65.8 and 60.0 at.% of Ru is present in its metallic state (BE at 462.0 ± 0.2 eV), respectively, for the $PtRu_{0.9}(CeO_2)_{0.1}$/C, $PtRu_{0.7}(CeO_2)_{0.3}$/C and $PtRu_{0.5}(CeO_2)_{0.5}$/C catalysts (see Fig. 4a–c). Furthermore, it should be mentioned that by incorporating the CeO_2 in the PtRu/C catalysts, the at.% of Ru in its oxidation state increases when compared with that of the unmodified PtRu/C catalysts (not shown). For instance, the at.% of Ru in its oxidation states (Ru(VI) at BE of 466.0 ± 0.04 eV) [25] increased from 29.1 to 40.0% when the CeO_2 content was increased from 0.1 to 0.5 at.% in the PtRu/C catalysts, which is relatively higher than the at.% of Ru oxides (20.46%) present in the unmodifeid PtRu/C catalyst (see Table 1). This is probably due to the preferable reaction of oxygen atoms released from the CeO_2 particles with unalloyed Ru particles present in the PtRu/C catalyst while annealing the catalyst under N_2 at 400 °C. Therefore, from the XPS results, it is clear that by increasing the at.% of CeO_2, the amount of ruthenium oxides increases in the PtRu/C catalyst accordingly.

Further, to see the chemical states of CeO_2 in all the ceria-based catalysts, the regional XPS spectrum for pure CeO_2/C, CeO_2-modified Pt/C and PtRu/C catalysts are presented in Fig. 5. In the spectrum of pure CeO_2/C, a couple of well-resolved components, namely $Ce3d_{5/2}$ and $Ce3d_{3/2}$ appeared.

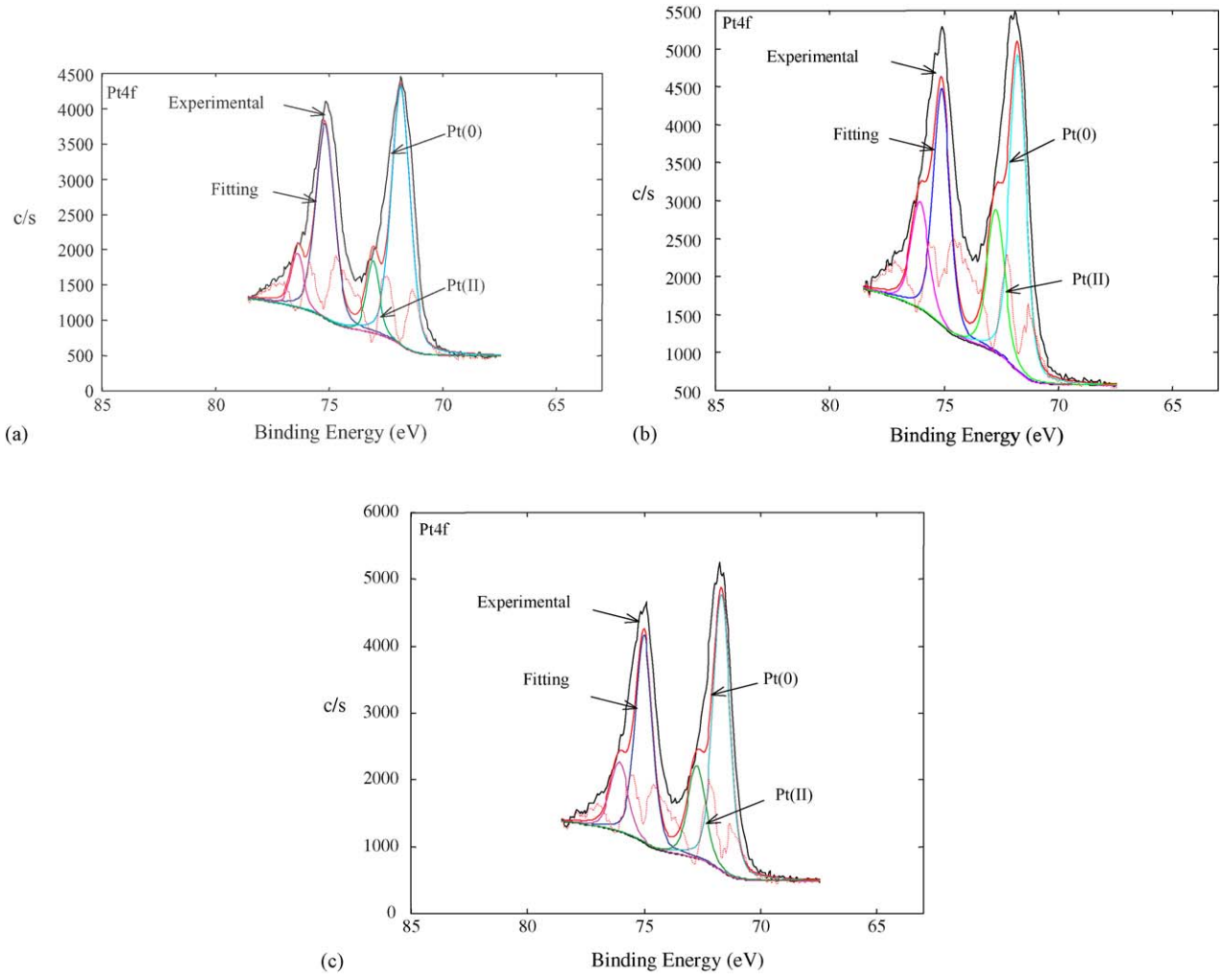

Fig. 3. Regional XPS spectrum of Pt4f: (a) $PtRu_{0.9}(CeO_2)_{0.1}$/C; (b) $PtRu_{0.7}(CeO_2)_{0.3}$/C; (c) $PtRu_{0.5}(CeO_2)_{0.5}$/C catalysts.

The component $Ce3d_{5/2}$ has two individual peaks at 882.5 and 886.0 eV and another component $Ce3d_{3/2}$ has three peaks at 898, 901 and 903.8 eV, which are in agreement with the data reported in the literature [26]. The existence of the two components with the above-mentioned peaks clearly indicates that the ceria is present in a mixed oxidation (Ce^{4+}–Ce^{3+}) states. Furthermore, an addition of CeO_2 in the Pt/C and PtRu/C catalysts did not make any shift in the binding energy positions of $Ce3d_{5/2}$ and $Ce3d_{3/2}$ components as compared with that of the pure CeO_2/C. This implies that not even a small amount of Pt or Ru was incorporated into the lattice of the CeO_2 in their ionic states.

3.4. Voltammetry

Fig. 6 shows the CV curves for the $Pt(CeO_2)$/C, PtRu/C, $PtRu_{0.9}(CeO_2)_{0.1}$/C, $PtRu_{0.7}(CeO_2)_{0.3}$/C and $PtRu_{0.5}(CeO_2)_{0.5}$/C catalysts in 0.5 M H_2SO_4 solution. For the PtRu/C catalyst, a single hydrogen desorption peak (curve b) is observed in the potential range from −0.25 to 0.05 V, which is consistent with the data reported in the literature [27]. On the other hand, for the $PtRu_{0.9}(CeO_2)_{0.1}$/C and $PtRu_{0.7}(CeO_2)_{0.3}$/C catalysts, a very broad hydrogen desorption peaks (curves c and d) are found in the potential range from −0.25 to 0.06 V. The formation of broad hydrogen desorption peaks can be attributed to the effect of enrichment of the Pt atoms in the $PtRu_{0.7}(CeO_2)_{0.3}$/C and $PtRu_{0.9}(CeO_2)_{0.1}$/C catalysts. The relatively higher Pt character than Ru in the $PtRu_{0.7}(CeO_2)_{0.3}$/C and $PtRu_{0.9}(CeO_2)_{0.1}$/C catalysts can be due to the effect of introduction of CeO_2 (0.1–0.3 at. wt.%) by replacing the Ru atoms in these catalysts. In addition, for the $PtRu_{0.7}(CeO_2)_{0.3}$/C and $PtRu_{0.9}(CeO_2)_{0.1}$/C catalysts, the double-layer charging current in the potential range from 0.05 to 0.4 V is found to be higher than that of the PtRu/C catalyst. This might be due to the formation of relatively higher amount of ruthenium hydroxide species ($Ru(OH)_x$) in the CeO_2-modified PtRu/C than that of PtRu/C catalysts. In the case of higher concentrated CeO_2-modified PtRu/C ($PtRu_{0.5}(CeO_2)_{0.5}$/C) and Pt catalysts, a very small hydrogen desorption peaks and double-layer charging current (see curves e and a) are observed. This can be attributed to the

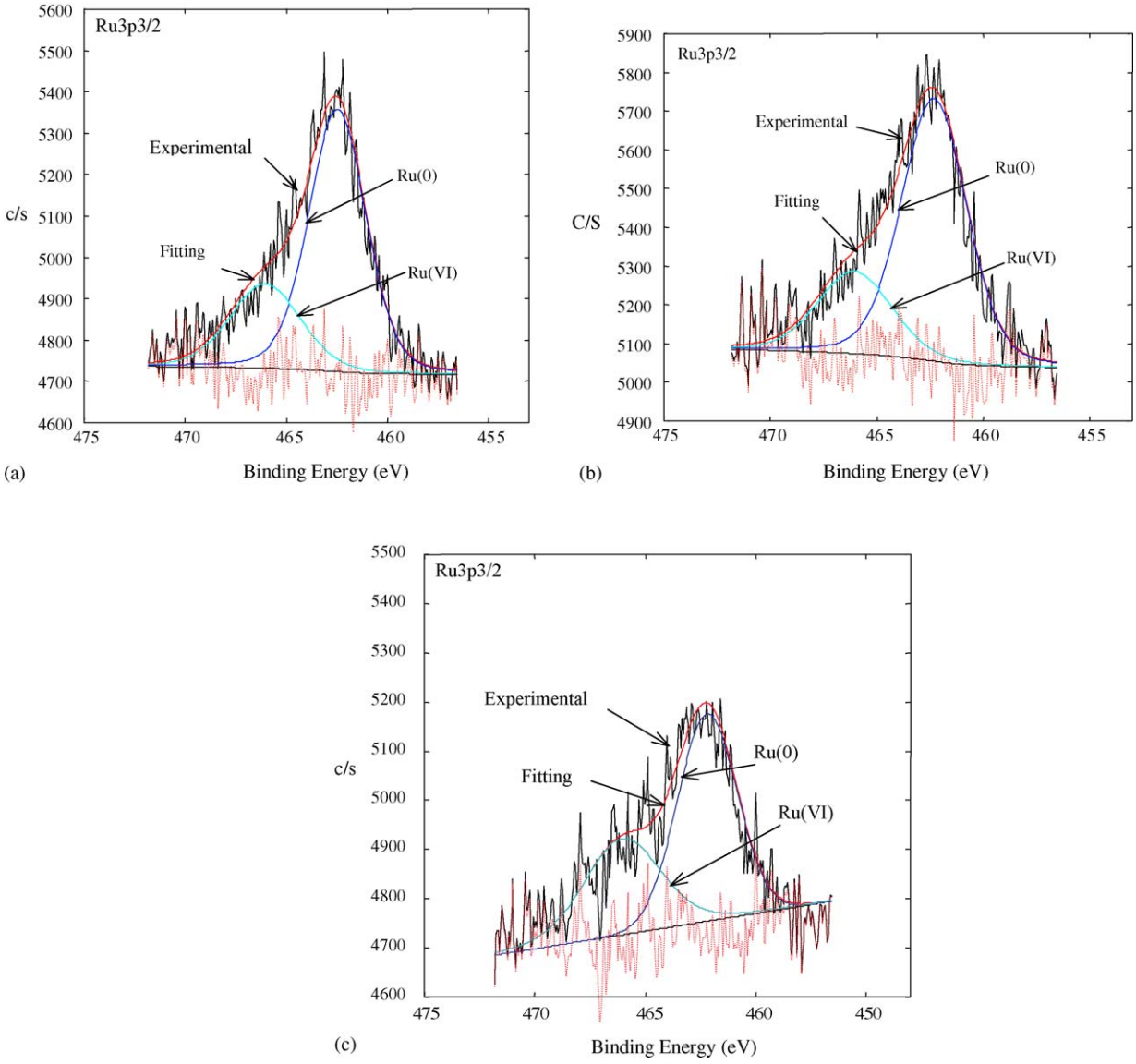

Fig. 4. Regional XPS spectrum of Ru3p3/2: (a) $PtRu_{0.9}(CeO_2)_{0.1}$/C; (b) $PtRu_{0.7}(CeO_2)_{0.3}$/C; (c) $PtRu_{0.5}(CeO_2)_{0.5}$/C catalysts.

agglomeration of PtRu and Pt particles in these catalysts as shown in the TEM images (see Fig. 1d and e).

Further, the electrochemical surface area (ESA) for the PtRu/C and CeO_2-modified Pt/C and PtRu/C catalysts was determined by integrating the charge of the hydrogen desorption region (Q_H) in the CV of Fig. 6 [28]. Assuming that the polycrystalline Pt electrode gives the hydrogen desorption charge of 0.21 mC cm^{-2}, we can obtain the ESA from [29]:

$$\text{ESA}\,(\text{m}^2\,\text{g}^{-1}\,\text{catalyst}) = \frac{Q_H}{0.21 \times 10^{-3}\,\text{C} \times \text{g catalyst}} \quad (1)$$

The calculated ESA values are given in Table 2. From Table 2, it is clear that the ESA values are very high for the $PtRu_{0.7}(CeO_2)_{0.3}$/C, $PtRu_{0.9}(CeO_2)_{0.1}$/C and PtRu/C catalysts because of the presence of relatively smaller size of Pt and Ru particles, in which hydrogen atoms can easily adsorb/desorb especially, on the surface of the Pt particles. On the other hand, the $PtCeO_2$/C and $PtRu_{0.5}(CeO_2)_{0.5}$/C catalysts exhibited very low ESA values because of the poor morphological structure of Pt particles in these catalysts as shown in Fig. 1d and e. It is interesting to note that for the $PtRu_{0.9}(CeO_2)_{0.1}$/C and $PtRu_{0.7}(CeO_2)_{0.3}$/C catalysts, the ESA values are not differed to a greater extent when compared with the PtRu/C catalyst, suggesting that the Pt particles were not oxidized/affected by the incorporation of CeO_2 in the PtRu/C catalysts as discussed in Sections 3.2 and 3.3.

Furthermore, we compared the methanol oxidation reactivity of the CeO_2-modified PtRu/C with that of the PtRu/C (both in-house and commercial) catalysts in 0.5 M H_2SO_4 solution. Fig. 7 shows the LSV curves for the in-house PtRu/C, E-TEK PtRu/C, $PtRu_{0.9}(CeO_2)_{0.1}$/C, $PtRu_{0.7}(CeO_2)_{0.3}$/C and $PtRu_{0.5}(CeO_2)_{0.5}$/C catalysts in 0.5 M H_2SO_4+2 M CH_3OH. For the in-house PtRu/C and

Table 1
Binding energies and atomic surface concentrations of different species obtained from XPS spectrum for the PtRu/C and CeO_2-modified PtRu/C catalysts

Catalyst	Peak	Binding energy (eV)	Species	Concentration (%)
PtRu/C	$Pt4f_{7/2}$	71.40	Pt(0)	82.34
		72.47	Pt(II)	17.66
	$Ru3p_{3/2}$	462.1	Ru(0)	79.54
		466.0	Ru(VI)	20.46
$PtRu_{0.9}(CeO_2)_{0.1}/C$	$Pt4f_{7/2}$	71.85	Pt(0)	83.98
		73.07	Pt(II)	16.02
	$Ru3p_{3/2}$	462.20	Ru(0)	70.90
		466.04	Ru(VI)	29.10
	$Ce3d_{5/2}$	885.0	Ce(IV)	–
	$Ce3d_{3/2}$	903.0	Ce(III)	–
$PtRu_{0.7}(CeO_2)_{0.3}/C$	$Pt4f_{7/2}$	71.78	Pt(0)	67.58
		72.73	Pt(II)	32.42
	$Ru3p_{3/2}$	462.07	Ru(0)	65.79
		464.87	Ru(VI)	34.21
	$Ce3d_{5/2}$	882.5	–	–
		886.0	Ce(IV)	–
	$Ce3d_{3/2}$	898.0	–	–
		901.0	Ce(III)	–
$PtRu_{0.5}(CeO_2)_{0.5}/C$	$Pt4f_{7/2}$	71.67	Pt(0)	73.88
		72.73	Pt(II)	26.12
	$Ru3p_{3/2}$	462.20	Ru(0)	60.0
		466.04	Ru(VI)	40.0
	$Ce3d_{5/2}$	885.0	Ce(IV)	–
	$Ce3d_{3/2}$	903.0	Ce(III)	–

E-TEK PtRu/C catalysts, the onset of methanol oxidation reaction took place around at 0.31 V, whereas for the $PtRu_{0.9}(CeO_2)_{0.1}/C$ and $PtRu_{0.7}(CeO_2)_{0.3}/C$ catalysts, the respective onset of methanol oxidation reaction occurred at 0.25 and 0.24 V, which is about 60 and 70 mV lower than the PtRu/C catalysts (see Table 2). In addition, the methanol oxidation current of the $PtRu_{0.7}(CeO_2)_{0.3}/C$ and $PtRu_{0.9}(CeO_2)_{0.1}/C$ catalysts is substantially higher than the PtRu/C catalysts in the potential region from 0.3 to 0.75 V. The in-house PtRu/C catalysts exhibited relatively a lower methanol oxidation current, despite it has comparable ESA value with that of the $PtRu_{0.7}(CeO_2)_{0.3}/C$ and $PtRu_{0.9}(CeO_2)_{0.1}/C$ catalysts. This might be due to the presence of lower amount of RuO_x (mediator species for the methanol oxidation reaction) in the PtRu/C, when compared with that of the $PtRu_{0.7}(CeO_2)_{0.3}/C$ and $PtRu_{0.9}(CeO_2)_{0.1}/C$ catalysts (see Table 1). The underlying mechanism for the

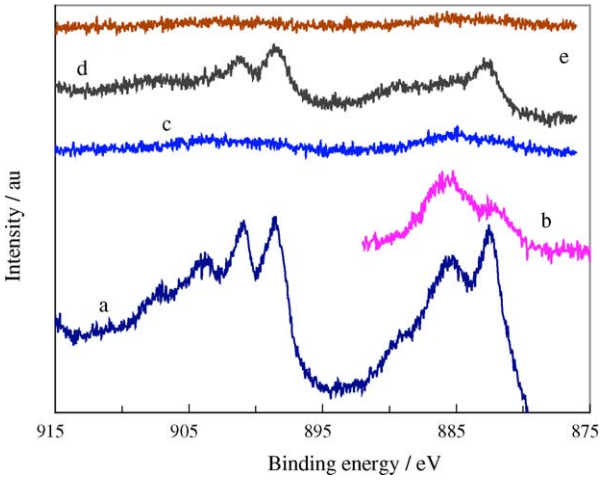

Fig. 5. Regional XPS spectrum of Ce3d: (a) CeO_2/C; (b) $Pt(CeO_2)/C$; (c) $PtRu_{0.9}(CeO_2)_{0.1}/C$; (d) $PtRu_{0.7}(CeO_2)_{0.3}/C$; (e) $PtRu_{0.5}(CeO_2)_{0.5}/C$ catalysts.

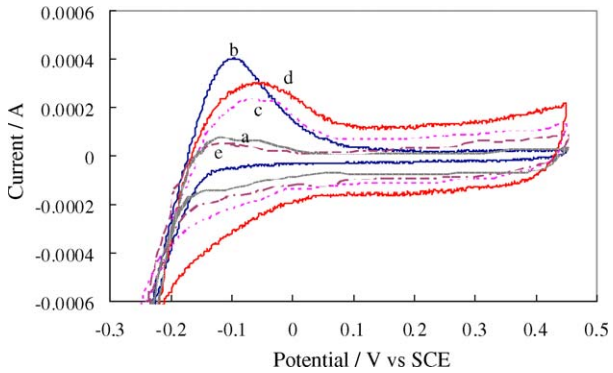

Fig. 6. CV curves for: (a) $Pt(CeO_2)/C$; (b) PtRu/C; (c) $PtRu_{0.9}(CeO_2)_{0.1}/C$; (d) $PtRu_{0.7}(CeO_2)_{0.3}/C$; (e) $PtRu_{0.5}(CeO_2)_{0.5}/C$ catalysts in 0.5 M H_2SO_4 solution.

Table 2
The ESA and onset potential for methanol oxidation for the PtRu/C and CeO_2-modified Pt/C and PtRu/C catalysts

Catalyst	Catalyst loading ($\mu g\,cm^{-2}$)	ESA ($m^2\,g^{-1}$)	Onset potential of methanol oxidation (V)
$PtCeO_2$/C	160	4.02	–
In-house PtRu/C	160	15.58	0.31
$PtRu_{0.9}(CeO_2)_{0.1}$/C	160	13.24	0.25
$PtRu_{0.7}(CeO_2)_{0.3}$/C	160	15.67	0.24
$PtRu_{0.5}(CeO_2)_{0.5}$/C	160	2.01	0.31

formation of relatively higher amount of RuO_x species in the CeO_2-modified PtRu/C catalysts will be discussed in the following section. Contrarily, in the case of $PtRu_{0.5}(CeO_2)_{0.5}$/C catalyst, no significant improvement in the methanol oxidation activity is observed as compared with that of the PtRu/C catalysts. The $PtRu_{0.7}(CeO_2)_{0.3}$/C catalyst gave the best performance for the methanol oxidation reaction among the CeO_2-modified PtRu/C catalysts. The possible mechanism leading to the lower onset potential and higher methanol oxidation current by using the $PtRu_{0.7}(CeO_2)_{0.3}$/C catalyst is discussed next.

As mentioned in discussing their XPS spectrum, when the $PtRu_{0.7}(CeO_2)_{0.3}$/C and $PtRu_{0.9}(CeO_2)_{0.1}$/C catalysts were annealed at 400 °C, the oxygen atoms released by the CeO_2 particles can easily react with some of the unalloyed surface Ru atoms because of their higher oxophilic character and form RuO_x species as indicated by the following reactions:

$$CeO_2 \rightarrow CeO_{2-x} + \frac{x}{2}O_2 \quad (2)$$

$$Ru + \frac{x}{2}O_2 \rightarrow RuO_x \quad (3)$$

The RuO_x species are likely to be involved in the mediation of the methanol oxidation as represented by

$$Pt + CH_3OH \rightarrow Pt\text{-}(CO)_{ads} + 4H^+ + 4e^- \quad (4)$$

$$Pt\text{-}(CO)_{ads} + RuO_x \rightarrow Pt + Ru + CO_2 + H^+ + e^- \quad (5)$$

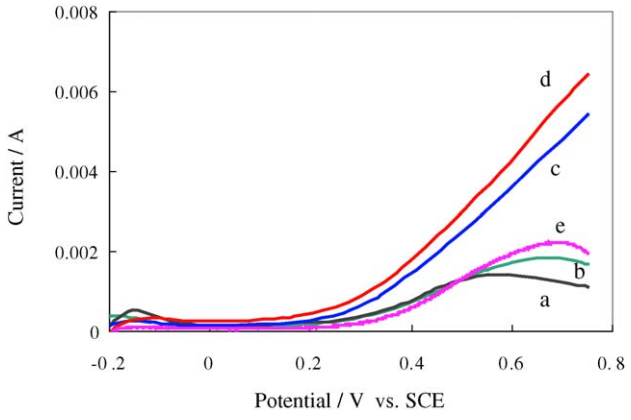

Fig. 7. LSV curves for: (a) E-TEK PtRu/C; (b) in-house PtRu/C; (c) $PtRu_{0.9}(CeO_2)_{0.1}$/C; (d) $PtRu_{0.7}(CeO_2)_{0.3}$/C; (e) $PtRu_{0.5}(CeO_2)_{0.5}$/C catalysts in 0.5 M H_2SO_4 + 2 M CH_3OH.

which take place in a relatively lower potential region (0.23 V versus SCE). In the $PtRu_{0.7}(CeO_2)_{0.3}$/C catalyst, the Ru atoms located in the adjacent Pt sites and the conversion of some of the unalloyed surface Ru atoms into RuO_x species as per reaction (3) might provide an optimal configuration of the catalytic particles and active oxygen atoms for the promotion of higher methanol oxidation reaction. On the other hand, in the case of $PtRu_{0.5}(CeO_2)_{0.5}$/C catalyst, although the higher amount of RuO_x species are formed (see Table 1), which is necessary for the mediation of methanol oxidation reaction, the poor morphological structure of this catalyst as discussed in the preceding section can mitigate the catalytic activity. Thus, it is inferred that in the $PtRu_{0.7}(CeO_2)_{0.3}$/C catalyst, the formation of RuO_x species induced by the CeO_2 as per reactions (2) and (3) can be involved in the mediation of methanol oxidation reaction, in addition to the $Ru(OH)_x$ species formed electrochemically through the discharge of water molecules on Ru atoms at about 0.31 V versus SCE.

$$Ru + H_2O \rightarrow Ru(OH)_x + H^+ + e^- \quad (6)$$

Therefore, from this preliminary investigation, although an optimal amount of CeO_2 could not be identified because of the difference in the morphological structure among the CeO_2-modified PtRu/C catalysts, it is clear that an addition of small amount of CeO_2 to replace Ru atoms in the PtRu(1:1)/C catalyst can strengthen the bi-functional mechanism, thereby, enhancing the methanol oxidation reaction.

3.5. Chronoamperometry

Fig. 8 shows the chronoamperometry curves for the in-house PtRu/C, E-TEK PtRu/C, $PtRu_{0.9}(CeO_2)_{0.1}$/C, $PtRu_{0.7}(CeO_2)_{0.3}$/C and $PtRu_{0.5}(CeO_2)_{0.5}$/C catalysts in 0.5 M H_2SO_4 solution containing 2 M CH_3OH at the potential of 0.4 V for 2000 s. For the $PtRu_{0.7}(CeO_2)_{0.3}$/C catalyst, the initial methanol oxidation current is relatively higher than the other catalysts, which is consistent with that of the LSV

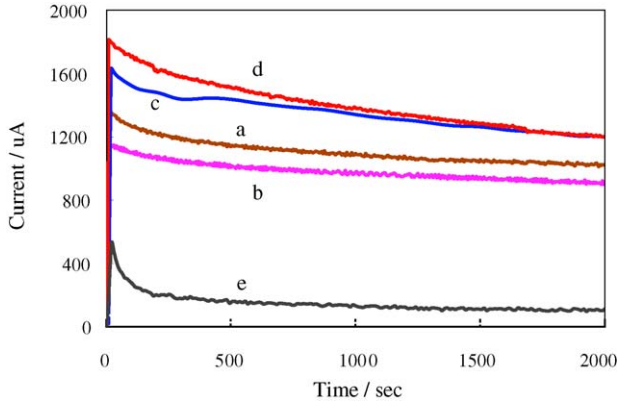

Fig. 8. Chronoamperometry curves for: (a) in-house PtRu/C; (b) E-TEK PtRu/C; (c) $PtRu_{0.9}(CeO_2)_{0.1}$/C; (d) $PtRu_{0.7}(CeO_2)_{0.3}$/C; (e) $PtRu_{0.5}(CeO_2)_{0.5}$/C catalysts in 0.5 M H_2SO_4 + 2 M CH_3OH at 0.4 V for 2000 s.

Table 3
The long-term poisoning rate for the CeO_2-modified PtRu/C and PtRu/C catalysts

Catalyst	Poisoning rate (δ % per s)
In-house PtRu/C	0.0044
E-TEK PtRu/C	0.0056
$PtRu_{0.9}(CeO_2)_{0.1}$/C	0.0101
$PtRu_{0.7}(CeO_2)_{0.3}$/C	0.0113
$PtRu_{0.5}(CeO_2)_{0.5}$/C	0.0093

results. As can be seen from Fig. 7, for all the catalysts, the methanol oxidation current gradually decayed with time, which was caused by the formation of intermediate species, such as CO_{ads}, CHO_{ads} and CH_3OH_{ads} species during the methanol oxidation reaction [30]. We calculated the long-term poisoning rate (δ) by measuring the linear decay of the current at times greater than 500 s from Fig. 8 [31]:

$$\delta = \frac{100}{I_0} \times \left(\frac{dI}{dt}\right)_{t>500\,s} (\%\ \text{per s}), \quad (7)$$

where $\left(\frac{dI}{dt}\right)_{t>500\,s}$ is the slope of the linear portion of the current decay and I_0 is the current at the start of polarization back extrapolated from the linear current decay. The calculated δ values are given in Table 3. Although the initial methanol oxidation current for the $PtRu_{0.9}(CeO_2)_{0.1}$/C and $PtRu_{0.7}(CeO_2)_{0.3}$/C catalysts is relatively higher than the PtRu/C catalysts, the long-term poisoning rate of the CeO_2-based PtRu/C catalysts is found to be almost double the value of the PtRu/C catalysts. This can be explained that in the Pt-enriched $PtRu_{0.7}(CeO_2)_{0.3}$/C and $PtRu_{0.9}(CeO_2)_{0.1}$/C catalysts, the RuO_x formed via the reaction (2) can remain as the source for the supply of active oxygen atoms, in addition to $Ru(OH)_x$ species (reaction (6)) for the oxidation of methanol species; due to that, the initial methanol oxidation current of $PtRu_{0.9}(CeO_2)_{0.1}$/C and $PtRu_{0.7}(CeO_2)_{0.3}$/C catalysts is found to be very high. After some time, although the methanol oxidation reaction is continuously mediated by the electrochemically formed $Ru(OH)_x$ species at the potential of 0.4 V, the supply of active oxygen atoms from the RuO_x species for the oxidation of methanol might be depleted due to the consumption of these oxygen atoms during the continuous process of the methanol oxidation reaction. This can lead to an accumulation of some intermediate species on the Pt atoms of the $PtRu_{0.9}(CeO_2)_{0.1}$/C and $PtRu_{0.7}(CeO_2)_{0.3}$/C catalysts, thereby, causing a decline in the methanol oxidation current. However, although the methanol oxidation current is rapidly declined for the $PtRu_{0.9}(CeO_2)_{0.1}$/C and $PtRu_{0.7}(CeO_2)_{0.3}$/C catalysts over the time, the overall methanol oxidation current on these catalysts is maintained at a higher level than the PtRu/C catalysts. For the $PtRu_{0.5}(CeO_2)_{0.5}$/C catalyst, a very low initial methanol oxidation current and more or less same level of poisoning rate as that of the $PtRu_{0.9}(CeO_2)_{0.1}$/C and $PtRu_{0.7}(CeO_2)_{0.3}$/C catalysts has been noted. This can be attributed to the poor morphological structure of this catalyst as discussed in the preceding sections.

4. Conclusions

In the present investigation, $PtRu_{0.9}(CeO_2)_{0.1}$/C, $PtRu_{0.7}(CeO_2)_{0.3}$/C and $PtRu_{0.5}(CeO_2)_{0.5}$/C catalysts were synthesized for the first time by using sodium borohydride as a reducing agent. The TEM images indicated that in the lower concentrated (0.1 and 0.3 at.%) CeO_2-modified PtRu/C catalysts, well-dispersed nanoparticles of size around 2.3–2.5 nm were formed on the carbon support. The XRD and XPS results indicated the formation of PtRu alloy and presence of ceria in an amorphous phase with Ce^{3+}–Ce^{4+} oxidation states. The LSV results demonstrated that the $PtRu_{0.7}(CeO_2)_{0.3}$/C catalyst exhibited a higher electro-catalytic activity for the methanol oxidation reaction than did the conventional PtRu/C catalysts. In the Pt-enriched $PtRu_{0.7}(CeO_2)_{0.3}$/C catalyst, the conversion of some of the unalloyed surface Ru atoms into RuO_x species, which can be induced by the CeO_2 particles, might provide an optimal configuration of the catalytic particles and active oxygen atoms for the higher methanol oxidation reaction. The $PtRu_{0.5}(CeO_2)_{0.5}$/C catalyst did not show a higher activity than did the other modified CeO_2 catalysts and this can be attributed to the poor morphological structure of this catalyst. The chronoamperometry results revealed that although the $PtRu_{0.7}(CeO_2)_{0.3}$/C and $PtRu_{0.9}(CeO_2)_{0.1}$/C catalysts yielded a higher methanol oxidation current, the long-term poisoning rate of these catalysts is found to be higher than the PtRu/C catalysts. During the long-term methanol oxidation reaction on the $PtRu_{0.7}(CeO_2)_{0.3}$/C and $PtRu_{0.9}(CeO_2)_{0.1}$/C catalysts, although the reaction is continuously mediated by the electrochemically formed $Ru(OH)_x$ species, the additional supply of active oxygen atoms from the RuO_x species might be depleted due to the continuous consumption of these oxygen atoms for the methanol oxidation reaction, which resulted in an increased poisoning rate on these catalysts.

Acknowledgements

The work described in this paper was supported by a grant from the Research Grants Council (Project No. HKUST6038/02E) and a grant from the Innovation and Technology Commission (Project No. ITS/069/02) of the Hong Kong SAR Government, China.

References

[1] A. Hamnett, Philos. Trans. R. Soc. Lond. Ser. A 354 (1996) 1653.
[2] A.K. Shukla, P.A. Christensen, A.J. Dickinson, A. Hammnet, J. Power Sources 76 (1998) 54.
[3] H. Yang, T.S. Zhao, Q. Ye, Electrochem. Commun. 6 (2004) 1098.
[4] Q. Ye, T.S. Zhao, H. Yang, J. Prabhuram, Electrochem. Solid-State Lett. 8 (1) (2005) 52.
[5] H. Yang, T.S. Zhao, Q. Ye, J. Power Sources 139 (1–2) (2004) 79.

[6] J. Prabhuram, T.S. Zhao, H. Yang, J. Electroanal. Chem. 578 (2005) 105.
[7] J.G. Liu, T.S. Zhao, R. Chen, C.W. Wong, Electrochem. Commun. 7 (2005) 288.
[8] H.A. Gasteiger, N. Markovic, P.N. Ross, E.J. Cairns, J. Phys. Chem. 97 (1993) 12020.
[9] M. Krausa, W. Vielstich, J. Electroanal. Chem. 379 (1994) 307.
[10] S.A. Arico, Z. Poltarzewski, H. Kim, A. Morana, N. Giordano, V. Antonucci, J. Power Sources 55 (1995) 159.
[11] K. Wang, H.A. Gasteiger, N. Markovic, P.N. Ross, Electrochim. Acta 41 (1996) 2587.
[12] M. Gotz, H. Wendt, Electrochim. Acta 43 (1998) 3637.
[13] G. Samjeske, H. Wang, T. Loffler, H. Baltruschat, Electrochim. Acta 47 (2002) 3681.
[14] K. Lasch, L. Jorissen, J. Garche, J. Power Sources 84 (1999) 225.
[15] Z. Jusys, T.J. Schmidt, L. Dubau, K. Lasch, L. Jorissen, J. Garche, R.J. Bhem, J. Power Sources 105 (2002) 297.
[16] L.X. Yang, C. Bock, B. MacDougall, J. Park, J. Appl. Electrochem. 34 (2004) 427.
[17] K.-W. Park, J.-H. Choi, K.-S. Ahn, Y.-E. Sung, J. Phys. Chem. B 108 (2004) 5989.
[18] C. Xu, P.K. Shen, J. Power Sources 142 (2005) 27.
[19] A. Holmgren, B. Andersson, J. Catal. 178 (1998) 14.
[20] J.W. Guo, T.S. Zhao, J. Prabhuram, C.W. Wong, Electrochim. Acta 50 (2005) 1973.
[21] J.W. Guo, T.S. Zhao, J. Prabhuram, R. Chen, C.W. Wong, Electrochim. Acta, in press.
[22] T. Masui, H. Hirai, R. Hamada, N. Imanaka, G. Adachi, T. Sakata, H. Mori, J. Mater. Chem. 13 (2003) 622.
[23] H.B. Yu, J.-H. Kim, H.-I. Lee, M.A. Schibioh, J. Lee, J. Han, S.P. Yoon, H.Y. Ha, J. Power Sources 140 (2005) 59.
[24] E.M. Crabb, R. Marshall, D. Thompsett, J. Electrochem. Soc. 147 (12) (2000) 4440.
[25] A.S. Arico, P. Creti, H. Kim, R. Mantegna, N. Giordano, V. Antonucci, J. Electrochem. Soc. 143 (12) (1996) 3950.
[26] S. Damyanova, J.M.C. Bueno, Appl. Catal. 253 (2003) 135.
[27] W.H. Lizcano-Valbuena, V.A. Paganin, E.R. Gonzalez, Electrochim. Acta 47 (2002) 3715.
[28] Z. Liu, J.Y. Lee, W. Chen, M. Han, L.M. Gan, Langmuir 20 (2004) 181.
[29] R. Woods, J. Electroanal. Chem. 9 (1976) 1.
[30] A. Kabbabi, R. Faure, R. Durand, B. Beden, F. Hahn, J.-M. Leger, C. Lamy, J. Electroanal. Chem. 444 (1998) 41.
[31] J. Jiang, A. Kucernak, J. Electroanal. Chem. 543 (2003) 187.